

A Flow-through Electrode for Superior Water Splitting by Mitigating Bubble Induced Overpotential

Yu Chen¹, Jiaojiao Chen¹, Ke Bai¹, Zeyi Xiao¹, and Senqing Fan¹

¹Sichuan University

November 26, 2022

Abstract

Bubble evolution induced overpotential for hydrogen production by water electrolysis is an important issue and the generated gas bubbles will cover the internal/external surface of the electrode. Herein, a flow-through electrode loaded with Co-based nanosheets is presented. Under the condition of flow-through mode, the catalysts can be adequately exposed because the generated bubbles can be timely removed from the catalyst surface. The overpotential can be reduced by about 100 mV for hydrogen evolution reaction (HER) and 57 mV for oxygen evolution reaction (OER) under the condition of 300 mA cm⁻² and electrolyte flux of 339 m³ m⁻² h⁻¹. A novel electrolyzer assembled with flow-through electrode for hydrogen production by alkaline water electrolysis is conducted. The cell voltage can be decreased by 100 mV at 400 mA cm⁻² at 6 M KOH, 338 K, and 1 atm, with the energy of 5 kWh Nm⁻³ required.

A Flow-through Electrode for Superior Water Splitting by Mitigating Bubble Induced Overpotential

Yu Chen, Jiaojiao Chen, Ke Bai, Zeyi Xiao, Senqing Fan*

School of Chemical Engineering, Sichuan University, No. 24 South Section 1, Yihuan Road, Chengdu, 610065, China

*Email: fansenqing86@scu.edu.cn. Tel/Fax: +86-028-85405220.

Abstract: Bubble evolution induced overpotential for hydrogen production by water electrolysis is an important issue and the generated gas bubbles will cover the internal/external surface of the electrode. Herein, a flow-through electrode loaded with Co-based nanosheets is presented. Under the condition of flow-through mode, the catalysts can be adequately exposed because the generated bubbles can be timely removed from the catalyst surface. The overpotential can be reduced by about 100 mV for hydrogen evolution reaction (HER) and 57 mV for oxygen evolution reaction (OER) under the condition of 300 mA cm⁻² and electrolyte flux of 339 m³ m⁻² h⁻¹. A novel electrolyzer assembled with flow-through electrode for hydrogen production by alkaline water electrolysis is conducted. The cell voltage can be decreased by 100 mV at 400 mA cm⁻² at 6 M KOH, 338 K, and 1 atm, with the energy of 5 kWh Nm⁻³ required.

Keywords: Flow-through electrode; water splitting; bubble detachment; superaerophobicity; electrolyzer.

1. Introduction

Water electrolysis for hydrogen (H₂) evolution has been considered to be one of the most promising strategies to facilitate “Carbon peak” and “Carbon neutrality”.^{1, 2} Currently, most researchers are focused on the development of state-of-the-art catalysts with high intrinsic activity to improve the water adsorption, activation, and splitting process.³⁻⁷ However, even for robust catalysts, the generated gas bubbles during the

hydrogen evolution process will cover the catalyst surface, which creates a dead area, restricts the mass transfer between electrolyte and catalysts, and causes an overpotential, especially under higher current density (hundreds of mA cm⁻²).⁸⁻¹⁰ Besides, for the electrodes with three-dimensional porous structures, the bubbles formed in electrode pores will get trapped in the porous structure and the uplifting bubbles in the electrode external surface will form continuous bubble curtains.¹¹⁻¹³ Thus, the contact between the electrolyte and the catalyst would be weakened, which inevitably gives rise to energy losses and decreases electrochemical conversion efficiencies. In order to overcome these problems, it is important to accelerate the detachment of the generated bubbles from the electrodes during water electrolysis for hydrogen evolution.

Generally, fabricating superaerophobic electrodes with nanostructure is an efficient strategy for gas bubble detachment.^{14, 15} For such a surface with nanostructure like nanosheets,^{16, 17} nanoarrays,¹⁸ and nanocones,¹⁹ the gas-liquid-solid interface is discontinuous, which reduces the adhesive force of the bubbles.^{20, 21} As a result, the bubbles can detach from the electrode surface timely with a small size. For example, an underwater superaerophobic pine-shaped Pt nanoarray electrode was presented by Sun's group.¹⁸ The adhesive force decreased by almost 13 times and the bubble size decreased by about 6 times can be obtained compared with the Pt plat electrode. Besides, in order to further accelerate the detachment of generated bubbles, introducing external fields to enhance the driving force of bubble detachment is an effective strategy. It has been reported that the performance of alkaline water electrolysis (AWE) by foam electrodes can be enhanced under the existence of a magnetic field.²² Besides, ultrasonic and supergravity fields have been also used to introduce convection for the rapid removal of gas bubbles to avoid bubbles covering the active site for a long time.²³⁻²⁵ However, the introduction of these external fields above inevitably increases the total equipment investment.

In order to avoid the introduction of additional equipment investment, flow-through electrodes would be a promising strategy for bubble detachment during hydrogen production by water electrolysis, since the directional movement of generated bubbles can be driven by the fluid flowing through the electrodes. Currently, there is a growing interest in the flow-through electrodes for performing electrochemical processes with enhanced mass transfer be achieved.²⁶⁻²⁸ Herein, a flow-through electrode with Co-based nanosheets immobilized on Ni foam is presented for promoting bubble detachment and enhancing mass transfer during water splitting. Firstly, the electrode's internal/external surface was immobilized with the nanosheet-shaped catalysts for increasing the roughness of electrode surface and weakening the adhesion of the gas bubbles. Then, the electrolyte was flowing through the prepared electrodes with interconnected pores and low permeation resistance. The electrolyte flux was controlled by a peristaltic pump and recirculated in the corresponding compartment of the cell (Figure S1). The enhanced hydrogen evolution performance and mechanism under the condition of electrolyte flowing through electrode has been investigated. In addition, the energy consumption of the electrolyzer assembled with flow-through electrodes was also studied.

2. Experimental materials and methods

2.1. Materials

The Ni foams with different pore sizes (35, 75, and 110 PPI) were purchased from Kunshan Ansu Electronic Materials Business. CoCl₂·6H₂O, NaBH₄, KOH, NaOH, acetone, and HCl were purchased from Chron Chemicals (Chengdu, China). All reagents used in experiments are analytical grade and used as received without further purification. All deionized water (DI) is treated with nitrogen to remove dissolved oxygen prior to use.

2.2. Preparation of CoB/Ni flow-through electrode

Before everything started, the Ni foam was pretreated first based on the subsequent steps. First of all, it was put into a 3 mol L⁻¹ HCl solution for 10 min to remove surface native oxides. Then it was placed in acetone for 10 min to degrease under ultrasonic conditions. Afterward, it was immersed in DI water for 10 min to clean further under ultrasonic conditions. Lastly, it was rinsed thoroughly with DI water and stored in DI water at room temperature for later use.

As shown in figure 1A, the active Co-based flow-through electrodes were prepared within two facile stages. First, CoB nanocatalysts were assembled on Ni foam after the flowing synthesis process.^{29, 30} In brief, cobalt salt aqueous (0.5 M) and NaBH₄ aqueous (1.0 M) were alternately flowing through the Ni foam pores. During the process, Co²⁺ and NaBH₄ can contact in Ni foam pores. As a result, CoB can be formed in Ni foam pores. The steps were repeated in 4 cycles. Next, the prepared CoB immobilized on the flow-through electrode was *in-situ* restructured after HER/OER activation.

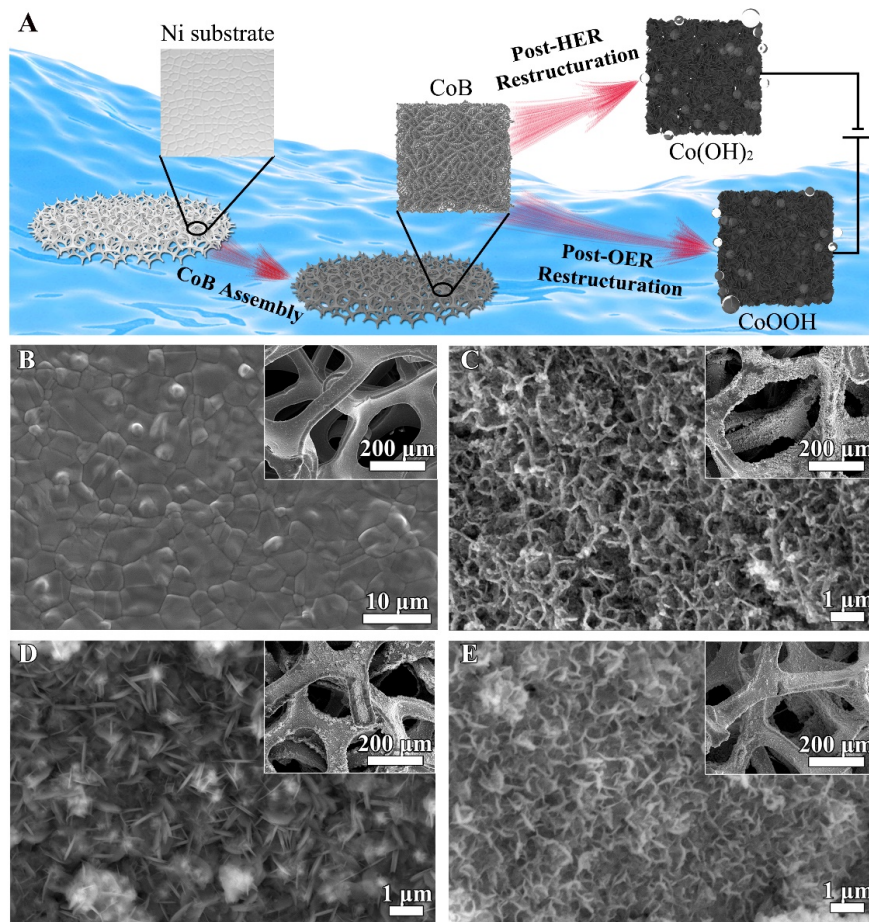


Figure 1. Illustration of the preparation of Co-based flow-through electrodes (A). The morphology of the pore surface of Ni foam (B), raw CoB/Ni flow-through electrode (C), and CoB/Ni flow-through electrode after HER activation (D) and OER activation (E).

2.3. Electrochemical measurements

Electrochemical measurements were performed in a custom two-compartment H-cell with cathode and anode compartments separated using an anion exchange membrane (AEM, Fumasep FAA-3-50) using a CHI 660E electrochemical workstation. A three-electrode configuration was employed with CoB/Ni flow-through electrode as the working electrode, Ti mesh coating with Pt as the counter electrode, and a Hg/HgO reference electrode, as shown in figure S1. Among those, the CoB/Ti membrane electrode was put in a self-made module with a module made of PTFE, a Ti ring as a current collector, and a silicone seal. The electrolyte flow rate was controlled by a peristaltic pump and recirculated in the corresponding compartment of the cell. We calculated the current density by electrode area (0.785 cm², based on the seal's inner diameter).

All measurements were performed at room temperature. The electrolyte (1 M KOH) was purged with dry N₂ 15 minutes before. All reported potentials were calibrated by an RHE based on the following equation:

The volume of H₂ and O₂ generated from cathode and anode cells was collected by the Drainage method. Before the hydrogen/oxygen evolution starts, the electrode was subjected to continuous CV scans until stabilized CV curves were observed. After electrochemical activation, the electrodes are named according to the active substance obtained by *in-situ* reconstitution.

2.4. Characterization

The electrochemical analysis and electrode characterization are shown in Supplementary Information.

3. Results and discussion

The morphologies of the flow-through electrode before and after HER/OER activation were characterized by SEM (Figure 1B-E). And the catalysts collected by treating flow-through electrodes under ultrasonic conditions were detected by TEM (Figure S2-S3). The Ni foam substrate shows an interconnected porous structure with a relatively smooth pore surface, as can be seen in Figure 1B. After the flowing synthesis of CoB nanocatalysts, CoB nanocatalysts can be uniformly immobilized in the pore surface of Ni foam without any blockage (Figure 1C). After further analysis by HAADF-STEM and elemental mapping, it can be seen that CoB nanoparticles were loaded on the nanosheet (Figure S2A) and the nanosheet was distributed with the element of Co, B, and O (Figure S3). Among these, the nanosheets obtained are probably derived from side reactions during the preparation of the catalyst. That is, Co²⁺ is precipitated as cobalt hydroxide nanosheets under alkaline conditions. Subsequently, after the CoB/Ni flow-through electrodes have been subjected to the HER/OER activation, the morphologies of nanocatalysts both changed. It can be seen in Figure 1D-F and Figure S2B-C, the nano CoB immobilized on the pore surface were completely transformed into the shape of nanosheets, which implies the active catalysts immobilized on the pore surface have been *in-situ* restructured.

For further investigation of the *in-situ* restructuration, the prepared flow-through electrodes before and after HER/OER activation have been tested by XPS (Figure 2A-C) and XRD (Figure S4). The surface chemical states of Co element for CoB/Ni were shown in Figure 2A, the Co 2p_{3/2} peak at 777.8 eV is assigned to Co⁰ in CoB, and the peaks at 781.2 eV are assigned to Co^{δ+} in CoO_x, which is resulted from the surface oxidation after the sample is exposed to air and water.³¹ The peak intensity of Co⁰ in CoB is relatively weak compared with that of Co^{δ+} in CoO_x, because the CoB was covered by surface oxidation species (Figure 2D). In addition, the same oxidation can also be found in the high-resolution spectrum of B 1s (Figure 2C). The XRD results (Figure S4) and the HRTEM image (Figure 2G) show that the prepared CoB on the pore surface is an amorphous compound. After HER/OER activation, the binding energy of Co 2p_{3/2} was shifted to low binding energy with a binding energy of 780.6 eV and 780.1 eV (Figure 2A), and the corresponding binding energy of O 1s for Co-OH (530.9 eV) and Co-O (529.3 eV) can be found (Figure 2B), while no signal can be found in high-resolution spectrum of B 1s (Figure 2C). Subsequently, the ICP-OES was used to detect the leaching amounts of flow-through electrode after HER/OER activation, as shown in Figure S5. The results show that the B element was completely leached out from CoB during the activation process. Eventually, the XRD results (Figure S4) and the HRTEM images (Figure 2H-I) of CoB/Ni after HER/OER furtherly proves that the active catalysts on the pore surface have been *in-situ* restructured into Co(OH)₂ and CoOOH, respectively. Hence, the prepared flow-through electrodes are named Co(OH)₂/Ni for HER and CoOOH/Ni for OER in the analysis and discussion.

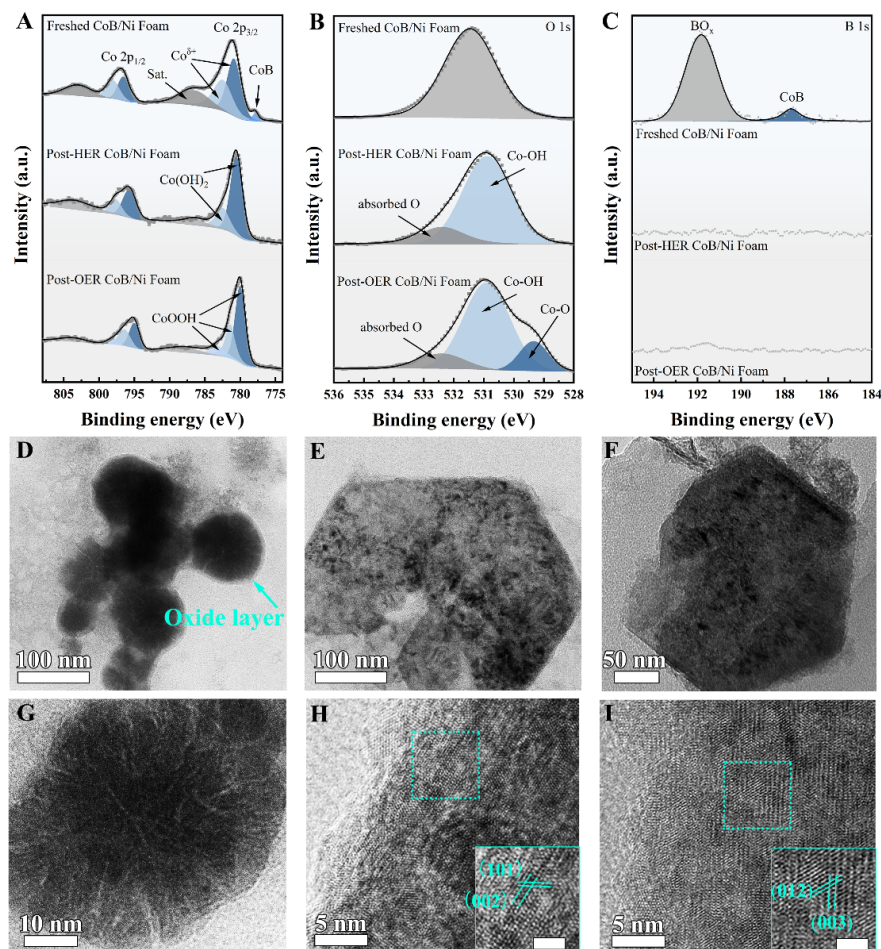


Figure 2. High-resolution spectra of Co (A), O 1s (B), and B 1s (C) of CoB/Ni flow-through electrode before and after HER/OER activation.

The AWE performance of each prepared electrode has been investigated in 1 M KOH solution. In this study, three different pore sizes of Ni foam have been chosen, with 35, 75, and 110 PPI. The thickness of each Ni foam is 1 mm, and the diameter of each Ni foam is 10 mm. The linear scan voltammetry (LSV) polarization curves (Figure 3A, Figure S6) were used to assess the performance of AWE at a scan rate of 5 mV s^{-1} . As can be seen, the catalytic performance can be enhanced after loading catalysts, with a reduction in the potential of almost 150 mV at 400 mA cm^{-2} . The best catalytic performance can be achieved by $\text{Co(OH)}_2/\text{Ni}$ electrode with a pore size of 75 PPI (Figure S7-S10), due to the largest electrochemical surface area (ECSA, 38.38 mF cm^{-2}) and the smallest reaction resistance (6.481 ohm).

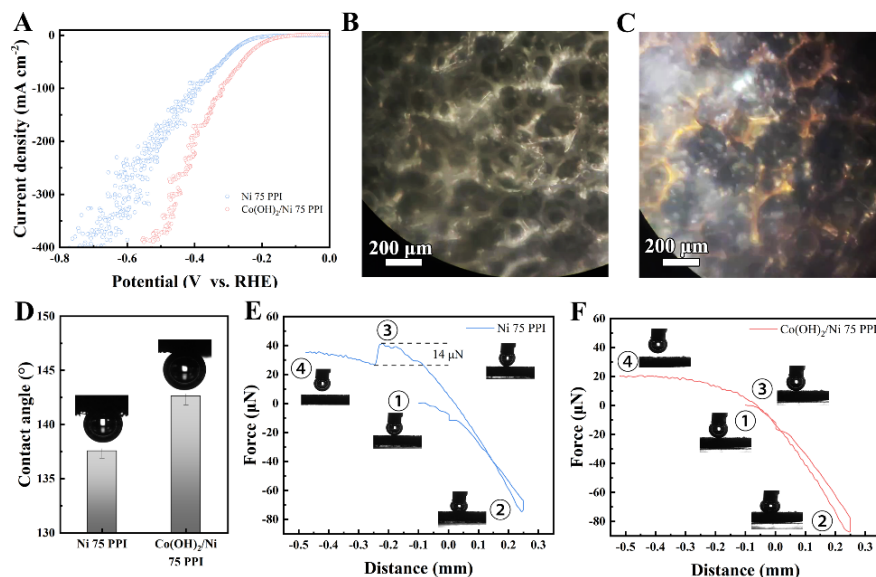


Figure 3. Polarization curves of Ni and $\text{Co(OH)}_2/\text{Ni}$ electrodes (A). Optical image of Ni foam (B), $\text{Co(OH)}_2/\text{Ni}$ (C) during hydrogen evolution (current density: 100 mA cm^{-2}), underwater H_2 bubble contact angle of Ni foam and $\text{Co(OH)}_2/\text{Ni}$ (D), H_2 bubble adhesive force measurements of Ni foam (E) and $\text{Co(OH)}_2/\text{Ni}$ (F) (insets: optical images of the H_2 bubble states in the corresponding position).

Gas evolution from the electrode surface usually brings disturbance to the electrode, which is reflected in the electrochemical curves. As can be seen in Figure 3A and S6, the curves show massive fluctuations as the current density increases. As can be seen in Figure 3B-C, the pore surface of the electrode can be covered by H_2 bubbles, severely reducing the catalytically active area of the electrode, and posing to decrease in current density. The catalytic sites can be re-exposed after generated bubble detaching, resulting in an instant increase in the current density. The fluctuations of LSV curves for $\text{Co(OH)}_2/\text{Ni}$ electrode are smaller than that of Ni electrode, which can be attributed to the microstructure change in the pore surface. It can be seen that, for Ni foam, the process of bubble nucleation to detachment takes 10 s (Figure S11) with an average bubble size of $47.76 \mu\text{m}$ (Figure S13A), at 10 mA cm^{-2} . However, after immobilizing nanosheet-shaped Co(OH)_2 catalysts, the residence time of H_2 bubble can be reduced to less than 1 s (Figure S12) with a smaller average bubble size of $23.13 \mu\text{m}$ (Figure S13B). The obvious decrease in bubble size can be attributed to the shortening of bubble growth time, which is satisfied with the bubble growth dynamic. In addition, the apparent difference in detachment behavior can also be observed in Video S1-S2 at 100 mA cm^{-2} . For Ni electrode, there exists an apparent bubble growth phase before it detaches, while for $\text{Co(OH)}_2/\text{Ni}$ electrode, the evolved bubbles can be directly detached from the electrode pores almost without any residence time can be observed. This phenomenon can be attributed to the difference in bubble adhesive force. It can be seen in Figure 3D, after immobilizing $\text{Co(OH)}_2/\text{Ni}$ catalysts in Ni pores, the underwater H_2 bubble contact angle rises from 137.5° to 142.5° , suggesting that loading Co(OH)_2 nanosheets on the pore surface improve the superaerophobicity which is beneficial to release H_2 bubbles. Meanwhile, the apparent bubble adhesive force of $14 \mu\text{N}$ and the apparent bubble transformation at position 3 can be found for Ni foam (Figure 3E), while no bubble adhesive force and bubble transformation can be found for Ni foam loaded with Co(OH)_2 nanosheets (Figure 3F). All those results prove that the adhesive force between bubbles and electrode active surface becomes lower after loading nanosheet-shaped catalysts. Hence, the generated H_2 bubbles can be timely detached from the electrode surface, and efficient and stable HER performance can be achieved.

The generated H_2 bubbles in electrode pores can be trapped in the pores (Figure S14B), although the enhanced bubble detachment behavior can be achieved by attenuating the adhesive force between bubbles and catalysts. Thus, the generated H_2 bubbles are difficult to remove out of pores timely, limiting the mass

transfer of electrolytes, eventually resulting in a decrease in electrochemical active sites. In addition, after the H₂ bubbles diffuse from pores to the electrode surface, a continuous H₂ bubble curtain can be formed on the electrode surface due to bubbles uplifting (inset image of Figure 4A), which also limits the mass transfer between the electrolyte and the catalytic sites in the electrode pores, especially under hundreds of current densities.

For accelerating the bubble detachment from the internal/external of the electrode, the prepared electrode was operated under the flow-through mode. In other words, the electrolytes were pumped through the electrode pores during the HER process (Figure S15). Figure 4A and Figure S16 show the polarization curves of the flow-through electrode under different fluxes. As can be seen, when the electrolyte was flowing through the electrode pores, the overpotential of HER became lower than that without electrolyte flows. It can be calculated that the potential of HER can be reduced more as the current densities increase (Figure 4B, Table S1). In this work, almost 130 mV potential can be reduced at 400 mA cm⁻², if the electrolyte flux was kept at 339 m³m⁻² h⁻¹. The obvious enhancement of HER performance can be attributed to the rapid removal of gas products (the residence time of H₂ bubbles was furtherly shortened to less than 0.1 s, as shown in Figure S17-S18). In this case, the bubbles formed at the pore surface and electrode external surface can be removed quickly with the electrolyte flow. Thus, the blockage of electrode pores (Figure S14D) and the formation of a bubble curtain (inset of Figure 4A) can be avoided, which enhanced the contact between electrolyte and electrode.

In addition, it can be found that the overpotential of HER can be affected by the flux of electrolytes (Figure 4C). The decreases in potential of HER were more obvious by increasing the flux of electrolytes flowing through the electrode pores. This result can be attributed to the shortening of the formed H₂ bubble residence time on the catalyst surface, which promotes the re-exposure of catalyst active sites. During the flow-through process, the generated bubbles are not only subject to adhesive force, gravity (G) and buoyancy (F_b), but also to the dragging force (F_d) caused by the electrolyte fluid flowing, as shown in Figure 4D-E. Thus, the residence time for the bubbles to detach from the pore surface mainly depends on the flux of the electrolyte. Higher flux could lead to a shorter residence time, since a greater dragging force can be generated under the condition of higher flux. Therefore, bubbles can be removed quickly from the micro-grade pores and re-exposing the catalyst active site and attenuating the negative effect of H₂ bubbles covered on the catalytic performance can be achieved.

Figure 4F, Figure S19 and S20 show the effects of electrolyte flux on current density. As can be seen in the chronoamperograms, the potential was set at -320, -400, -460, and -520 mV vs RHE, the initial values of current densities were corresponding to 100, 200, 300, and 400 mA cm⁻² in the absence of electrolyte flowing. During the test progress, the electrolyte flux was increased every 500 s. It can be found that at each current density, the current density of HER can be gradually increased by continuously increasing the flux of electrolytes. Besides, a graph of plotting increases in current density versus current density at a flux of 339 m³ h⁻¹m⁻² can be seen in Figure S21. The scattering point shows a good positive linear correlation. The results show that around a 10% increase in current density can be achieved by introducing electrolytes flowing in electrode pores at the same operating voltage. Meanwhile, the H₂ production also shows the same increase amount, and a close to 100% faraday efficiency can be achieved (Figure S22). In other words, more hydrogen production can be obtained for the same energy consumption conditions under the condition of electrolyte flows through the electrode pores.

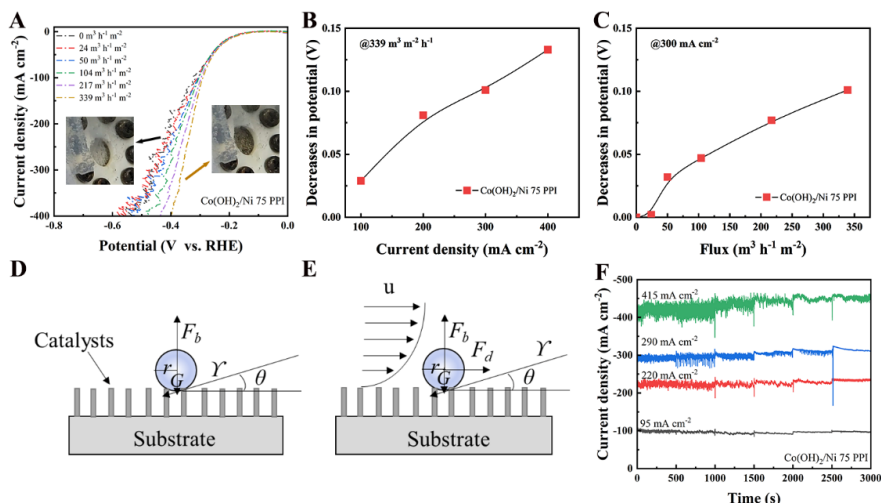


Figure 4. Electrochemical analysis of Ni and $\text{Co(OH)}_2/\text{Ni}$ flow-through electrodes with different pore sizes for HER electrocatalysis with flows. LSV curves (A) for $\text{Co(OH)}_2/\text{Ni}$ flow-through electrode with a pore size of 75 PPI under different flux, insets are optical images of the electrode surface with flows (right) and without flows (left). Decreases in potential under different current densities (B), different flux (C), and decreases in potential were calculated from the difference between the potential in the flowing and non-flowing cases. Schematic diagram of the force analysis of bubbles on the electrode surface without flows (D) and with flows (E). Chronoamperograms of $\text{Co(OH)}_2/\text{Ni}$ flow-through electrodes with a pore size of 75 PPI under different current densities and different flux, the flux is increased every 500 s (F).

As another gas evolution reaction of AWE, OER performance is also subject to the generated O_2 bubble. Figure 5A shows the LSV curves of OER under the condition of electrolytes flowing electrode pores. Similar trends can be found that the potential of OER can be decreased as the electrolyte flux increases, but the decreased values (Figure 5B-C) are less than that of the HER process. Similarly, the current density can be increased as the electrolyte flux increases (Figure S23, Table S2), but the current density increments (Figure 5D) in the OER process are less than that of the HER process. This can be attributed to two factors: For one thing, OER is a 4-electron transfer process and HER is a 2-electron transfer process. At the same current density, the O_2 product is half of H_2 . Hence the masking of the catalytic active sites caused by generated bubbles is not as severe as in the HER process. In other words, the effect of O_2 evolution process on electrode performance is weaker. For another thing, compared with lower H_2 solubility (1.8 vol% at 293 K), higher O_2 solubility (3.1 vol% at 293 K) leads to a lesser gas evolution amount. As a result, the decrease in potential for OER by flowing electrolyte through electrode pores is less, compared with that of HER.

The durability of $\text{Co(OH)}_2/\text{Ni}$ cathode and CoOOH/Ni anode was investigated (Figure 5E) by performing a long term catalytic test at 300 mA cm^{-2} . It can be found that both cathode and anode show excellent catalytic stability without any reduction in current density and no catalyst shedding was observed during a continued test for 18 hours. This can be mainly attributed to the advantages of the electrode preparation method, where unstable catalysts within the electrode pores can be removed with the continuous flushing of the precursor fluid during flowing synthesis. In addition, it was also found that the current density during the HER/OER process could be changed in time as the pump was switched on and off, demonstrating good instantaneous responsiveness.

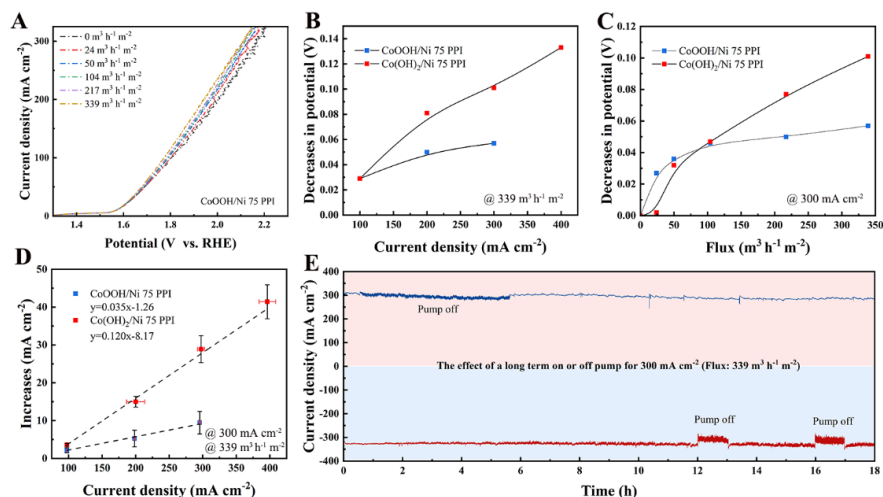


Figure 5. LSV curves (A) for CoOOH/Ni flow-through electrode with a pore size of 75 PPI under different flux. Decreases in potential under different current densities (B) and different flux (C) compared with that of HER. Increases in current density (D) at different current densities compared with that of HER. Durability of HER and OER process.

A novel electrolyzer assembled with flow-through electrode for AWE under high current density was also conducted with the results illustrated in Figure 6A and Figure S24. The AWE process was assessed at 6 M KOH, 338 K, and 1 atm, and the cell voltage is limited to 3 V to prevent excessive oxidation of the Ti current collector. The electrolyte was flowed through the electrode pores and recirculated in the corresponding compartment of the cell by peristaltic pumps. As can be seen in Figure 6B, the cell voltage can be decreased as the electrolyte flux rises from 22.5 m³ m⁻² h⁻¹ to 195 m³ m⁻² h⁻¹, which can be attributed to the rapid detachment of generated H₂/O₂ bubbles reducing the bubble induced overpotential. The degree of cell voltage reduction becomes larger with the increasing current density under the condition of electrolytes flowing through electrode pores. For Ni foam immobilized nanosheet-shaped Co-based catalysts, the cell voltage can be reduced from 2.92 V to 2.78 V at 1000 mA cm⁻² (Table S3), and the corresponding consumption can be reduced by approximately 0.55 kWh Nm⁻³. Compared with the electrolyzer by introducing other external fields, the cell voltage of flow-through electrolyzer is lower (Figure 6C). In addition, it is worth to notice that the energy consumption of 5 kWh Nm⁻³ can be achieved at 400 mA cm⁻² at 6 M KOH, 338 K, and 1 atm (Figure S25), without any noble metals (Pt, Ir, Ru) added as well as any complicated catalyst (high entropy alloys, single-atom catalysts) preparation processes. The energy required for AWE could be reduced more in this novel electrolyzer assembled with flow-through electrode, if AWE is conducted under the real industrial conditions with higher pressure and higher temperature, or immobilized state-of-the-art catalysts with better catalytic activity on flow-through electrodes.

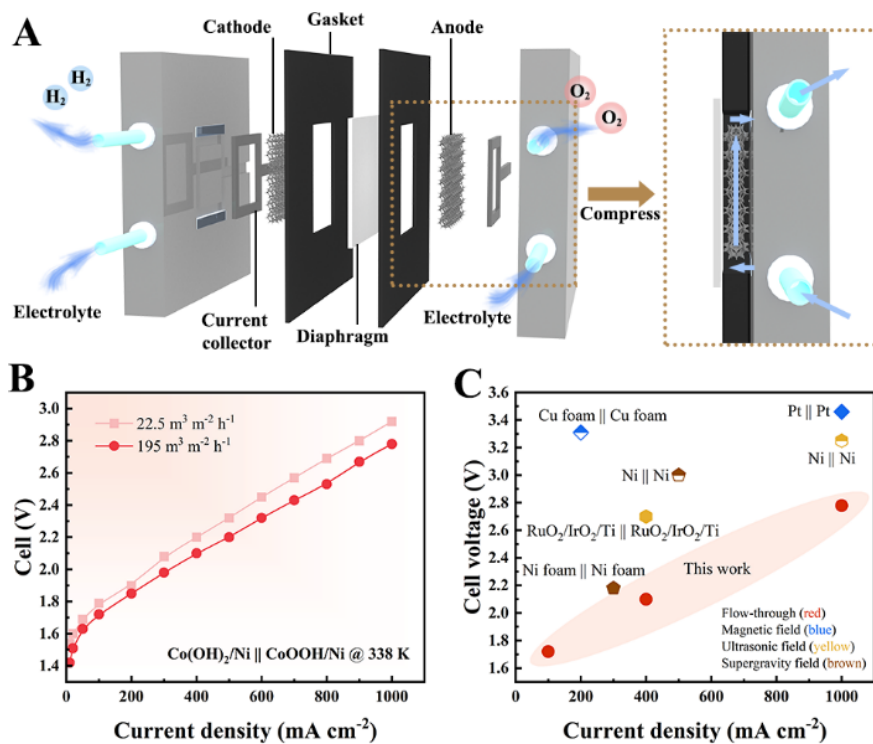


Figure 6. Schematic of flow-through electrolyzer (A). Cell voltage (B) vs current density curves for AWE by Co(OH)₂/Ni || CoOOH/Ni under the condition of electrolyte flowing through the electrode pores. Comparisons of cell voltage under various external fields (C).

4. Conclusions

In summary, we developed a two-step strategy for enhancing the performance of water splitting by attenuating the bubble evolution induced overpotential. First, a rough surface with superaerophobicity was fabricated to attenuate the bubble adhesive force by immobilizing nanosheet-shaped catalysts on Ni foam pores. Then, flow field was introduced to accelerate the bubble detachment and enhance the contact between catalysts and electrolyte. As a result, the obvious enhancement of HER/OER performance can be achieved under the condition of electrolyte flowing through the electrode pores. Besides, an assessment of electrolyzer assembled with flow-through electrodes was also proposed. The energy consumption of 5 kWh Nm⁻³ can be achieved at industrial current density (over hundreds of current density). However, it is worth noticing our flow-through electrodes have not immobilized those state-of-the-art catalysts. Hence, there remains room for further performance improvements. Finally, we posit that this strategy can be applied not only for water splitting, but also for those gas evolution reactions involved to improve electrochemical performance.

Acknowledgements

The present work was supported by the PetroChina Innovation Foundation (2021DQ02-0601) and the Science and technology leading talent cultivation project of Sichuan University (No. 0082604151335).

Conflict of interest

The authors declare no conflict of interest.

Reference

1. Li Y, Wei X, Chen L, and Shi J. Electrocatalytic Hydrogen Production Trilogy. *Angew. Chem. Int. Ed.* 2021; 60 (36): 19550-19571.

2. Kou T, Wang S, and Li Y. Perspective on High-Rate Alkaline Water Splitting. *ACS Mater. Lett.* 2021; 3 (2): 224-234.
3. Seh ZW, Kibsgaard J, Dickens CF, Chorkendorff I, Norskov JK, and Jaramillo TF. Combining theory and experiment in electrocatalysis: Insights into materials design. *Science.* 2017; 355 (6321): eaad4998
4. Hsu S-H, Hung S-F, Wang H-Y, Xiao F-X, Zhang L, Yang H, Chen HM, Lee J-M, and Liu B. Tuning the Electronic Spin State of Catalysts by Strain Control for Highly Efficient Water Electrolysis. *Small Methods.* 2018; 2 (5): 1800001.
5. Jothi VR, Karuppasamy K, Maiyalagan T, Rajan H, Jung CY, and Yi SC. Corrosion and Alloy Engineering in Rational Design of High Current Density Electrodes for Efficient Water Splitting. *Adv. Energy Mater.* 2020; 10 (24): 1904020.
6. Caban-Acevedo M, Stone ML, Schmidt JR, Thomas JG, Ding Q, Chang HC, Tsai ML, He JH, and Jin S. Efficient hydrogen evolution catalysis using ternary pyrite-type cobalt phosphosulphide. *Nat. Mater.* 2015; 14 (12): 1245-51.
7. Lu X and Zhao C. Electrodeposition of hierarchically structured three-dimensional nickel-iron electrodes for efficient oxygen evolution at high current densities. *Nat. Commun.* 2015; 6: 6616.
8. Jeon D, Park J, Shin C, Kim H, Jang J-W, Lee DW, and Ryu J. Superaerophobic hydrogels for enhanced electrochemical and photoelectrochemical hydrogen production. *Sci. Adv.* 2020; 6: eaaz3944
9. Wang JG, Shi L, Su Y, Liu L, Yang Z, Huang R, Xie J, Tian Y, and Li D. In-situ plasmonic tracking oxygen evolution reveals multistage oxygen diffusion and accumulating inhibition. *Nat. Commun.* 2021; 12 (1): 2164.
10. Angulo A, van der Linde P, Gardeniers H, Modestino M, and Fernández Rivas D. Influence of Bubbles on the Energy Conversion Efficiency of Electrochemical Reactors. *Joule.* 2020; 4 (3): 555-579.
11. Wang L, Huang X, Jiang S, Li M, Zhang K, Yan Y, Zhang H, and Xue JM. Increasing Gas Bubble Escape Rate for Water Splitting with Nonwoven Stainless Steel Fabrics. *ACS Appl. Mater. Interfaces.* 2017; 9 (46): 40281-40289.
12. Beck VA, Ivanovskaya AN, Chandrasekaran S, Forien JB, Baker SE, Duoss EB, and Worsley MA. Inertially enhanced mass transport using 3D-printed porous flow-through electrodes with periodic lattice structures. *Proc. Natl. Acad. Sci. U. S. A.* 2021; 118 (32).
13. Yang W and Chen S. Recent progress in electrode fabrication for electrocatalytic hydrogen evolution reaction: A mini review. *Chem. Eng. J.* 2020; 393.
14. Bae M, Kang Y, Lee DW, Jeon D, and Ryu J. Superaerophobic Polyethyleneimine Hydrogels for Improving Electrochemical Hydrogen Production by Promoting Bubble Detachment. *Adv. Energy Mater.* 2022; 12 (29): 2201452-9.
15. Shen J, Li J, Li B, Zheng Y, Bao X, Guo J, Guo Y, Lai C, Lei W, Wang S, and Shao H. Ambient Fast Synthesis of Superaerophobic/Superhydrophilic Electrode for Superior Electrocatalytic Water Oxidation. *Energy Environ. Mater.* 2022.
16. Guo Y, Yao Z, Shang C, and Wang E. Amorphous Co₂B Grown on CoSe₂ Nanosheets as a Hybrid Catalyst for Efficient Overall Water Splitting in Alkaline Medium. *ACS Appl. Mater. Interfaces.* 2017; 9 (45): 39312-39317.
17. Chang S, Zhang Y, Zhang B, Cao X, Zhang L, Huang X, Lu W, Ong CYA, Yuan S, Li C, Huang Y, Zeng K, Li L, Yan W, and Ding J. Conductivity Modulation of 3D-Printed Shellular Electrodes through Embedding Nanocrystalline Intermetallics into Amorphous Matrix for Ultrahigh-Current Oxygen Evolution. *Adv. Energy Mater.* 2021; 11 (28): 2100968.

18. Li Y, Zhang H, Xu T, Lu Z, Wu X, Wan P, Sun X, and Jiang L. Under-Water Superaerophobic Pine-Shaped Pt Nanoarray Electrode for Ultrahigh-Performance Hydrogen Evolution. *Adv. Funct. Mater.* 2015; 25 (11): 1737-1744.
19. Ge K, Zeng Y, Dong G, Zhao L, Wang Z, and Huang M. 3D self-standing grass-like cobalt phosphide vesicles-decorated nanocones grown on Ni-foam as an efficient electrocatalyst for hydrogen evolution reaction. *Int. J. Hydrogen Energy.* 2019; 44 (26): 13490-13501.
20. Lu Z, Zhu W, Yu X, Zhang H, Li Y, Sun X, Wang X, Wang H, Wang J, Luo J, Lei X, and Jiang L. Ultrahigh hydrogen evolution performance of under-water "superaerophobic" MoS(2) nanostructured electrodes. *Adv. Mater.* 2014; 26 (17): 2683-7, 2615.
21. Lu Z, Sun M, Xu T, Li Y, Xu W, Chang Z, Ding Y, Sun X, and Jiang L. Superaerophobic electrodes for direct hydrazine fuel cells. *Adv. Mater.* 2015; 27 (14): 2361-6.
22. Liu Y, Pan L-m, Liu H, Chen T, Yin S, and Liu M. Effects of magnetic field on water electrolysis using foam electrodes. *Int. J. Hydrogen Energy.* 2019; 44 (3): 1352-1358.
23. Swiegers GF, Terrett RNL, Tsekouras G, Tsuzuki T, Pace RJ, and Stranger R. The prospects of developing a highly energy-efficient water electrolyser by eliminating or mitigating bubble effects. *Sustainable Energy Fuels.* 2021; 5 (5): 1280-1310.
24. Wang M, Wang Z, Gong X, and Guo Z. The intensification technologies to water electrolysis for hydrogen production – A review. *Renewable Sustainable Energy Rev.* 2014; 29: 573-588.
25. Darband GB, Aliofkhaezrai M, and Shanmugam S. Recent advances in methods and technologies for enhancing bubble detachment during electrochemical water splitting. *Renewable Sustainable Energy Rev.* 2019; 114.
26. Chen J, Fan S, Chen Y, Wang Y, Bai K, Mai Z, and Xiao Z. Electrocatalytic Composite Membrane with Deep-Permeation Nano Structure Fabricated by Flowing Synthesis for Enhanced Catalysis. *J. Membr. Sci.* 2021; 636: 119616-10.
27. Vedharathinam V, Qi Z, Horwood C, Bourcier B, Stadermann M, Biener J, and Biener M. Using a 3D Porous Flow-Through Electrode Geometry for High-Rate Electrochemical Reduction of CO₂ to CO in Ionic Liquid. *ACS Catal.* 2019; 9 (12): 10605-10611.
28. Buffa A, Erel Y, and Mandler D. Carbon Nanotube Based Flow-Through Electrochemical Cell for Electroanalysis. *Anal. Chem.* 2016; 88 (22): 11007-11015.
29. Chen Y, Fan S, Qiu B, Chen J, Mai Z, Wang Y, Bai K, and Xiao Z. Cu-Ag Bimetallic Core-shell Nanoparticles in Pores of a Membrane Microreactor for Enhanced Synergistic Catalysis. *ACS Appl. Mater. Interfaces.* 2021; 13 (21): 24795-24803.
30. Chen Y, Fan S, Chen J, Deng L, and Xiao Z. Catalytic Membrane Nanoreactor with Cu-Ag_x Bimetallic Nanoparticles Immobilized in Membrane Pores for Enhanced Catalytic Performance. *ACS Appl. Mater. Interfaces.* 2022; 14 (7): 9106-9115.
31. Sun H, Xu X, Yan Z, Chen X, Jiao L, Cheng F, and Chen J. Superhydrophilic amorphous Co-B-P nanosheet electrocatalysts with Pt-like activity and durability for the hydrogen evolution reaction. *J. Mater. Chem. A.* 2018; 6 (44): 22062-22069.